HHS Public Access

Author manuscript

*Nanoscale*. Author manuscript; available in PMC 2019 November 29.

Published in final edited form as:

*Nanoscale*. 2018 November 29; 10(46): 21640–21647. doi:10.1039/c8nr05323e.

# BSA-bioinspired gold nanorods loaded with immunoadjuvant for treatment of melanoma by combined photothermal therapy and immunotherapy

**Benqing Zhou**[a,b], **Jun Song**[a], **Meng Wang**[a,b], **Xin Wang**[a], **Jielin Wang**[b], **Eric W. Howard**[c], **Feifan Zhou**[a,b], **Junle Qu**[a], and **Wei R. Chen**[b]

[a.]Key Laboratory of Optoelectronic Devices and Systems of Ministry of Education/Guangdong Province, College of Optoelectronic Engineering, Shenzhen University, Shenzhen, 518060, P. R. China

[b.]Biophotonics Research Laboratory, Center of Interdisciplinary Biomedical Education and Research, College of Mathematics and Science, University of Central Oklahoma, Edmond, Oklahoma, 73034, USA

[c.]Department of Cell Biology, University of Oklahoma Health Sciences Center, Oklahoma City, 73104, USA

## Abstract

Developing therapeutic methods that can effectively delay tumor growth, inhibit tumor metastases, and protect the host from tumor recurrence still faces challenges. Nanoparticle-based combination therapy may provide an effective therapeutic strategy. Herein, we show that bovine serum albumin (BSA)-bioinspired gold nanorods (GNRs) loaded with immunoadjuvant for combined photothermal therapy (PTT) and immunotherapy for treatment of melanoma. In this work, cetyltrimethylammonium bromide (CTAB) coated GNRs were successively decorated with polyethylene glycol (PEG) and BSA, and loaded with an immunoadjuvant imiquimod (R837). The synthesized *m*PEG-GNRs@BSA/R837 nanocomplexes under near-infrared (NIR) irradiation could effectively kill tumors and trigger strong immune responses in treating metastatic melanoma in mice. Furthermore, the nanocomplex-based PTT prevented lung metastasis and induced a strong long-term antitumor immunity to protect treated mice from tumor recurrence. The nanocomplex-based PTT in combination with immunotherapy may be potentially employed as an effective strategy for the treatment of melanoma and other metastatic cancers.

## Summary

A novel BSA-bioinspired gold nanorods loaded with immunoadjuvant is fabricated to combine photothermal therapy with immunotherapy for treatment of melanoma.

Conflicts of interest

There are no conflicts to declare.

Electronic Supplementary Information (ESI) available: Additional experimental results. See DOI: 10.1039/c8nr05323e

## Introduction

Melanoma is the fifth most common cancer in the United States, with an increased incidence rate over the past several decades.[1, 2] About 87,110 cases of melanoma were expected to be diagnosed in 2017.[1] Although the five-year survival rate for melanoma patients increased from 82% in 1975 to 93% in 2010, the overall mortality rate remained unchanged, primarily due to tumor metastasis, which continues to be a significant therapeutic challenge.[3]

Melanoma is one of the most immunogenic solid tumors. Immunotherapy appears to be a viable treatment option for melanoma, as most traditional cancer treatment modalities have low efficiency in most cases.[4-6] The most important milestone was the development of immune checkpoint inhibitors.[7-10] Since 2011, the Food and Drug Administration (FDA) has approved several novel agents including anti-programmed death 1 (PD1), anti-cytotoxic T-lymphocyte antigen-4 (CTLA-4), and peginterferon-α-2b, for the treatment of advanced melanoma.[11-14] However, the use of these new agents alone still displays low efficacy in treating advanced melanoma. An ideal cancer therapy should not only destroy the primary tumors, but also trigger host immune system to recognize, trace, and attack all remaining tumor cells, at either the site of the primary tumors or the site of distant metastases.[15-18] In view of these desirable properties, novel combinations of immunotherapy and other therapies, such as chemotherapy, photodynamic therapy, and photothermal therapy (PTT), have been developed to overcome the low response rates of immunotherapy and short-term effects of other therapies.[19-22]

Nanomaterials could realize the combination of immunotherapy and other therapies in virtue of their multifunction and optical/magnetic properties.[23-27] For example, poly(lactic-co-glycolic) acid (PLGA) encapsulated indocyanine green (ICG, a photothermal agent), and imiquimod (R837, an FDA approved immunomodulator through the toll-like receptor 7) was synthesized and applied for cancer PTT and immunotherapy.[28] Upconversion nanoparticles (UCNPs) had their application in loading chlorine e6 (Ce6, a photosensitizer for photodynamic therapy) and R837 immunoadjuvant.[25] The designed UCNPs-Ce6-R837 performed well in suppressing colorectal cancer and resistance of tumor reoccurrence. Single-walled carbon nanotube (SWNTs) conjugated to glycated chitosan (GC, a immunoadjuvant) showed great antitumor efficiency in inhibiting tumor growth, prolonging survival time, and preventing tumor recurrence.[29] Among these nanomaterials, gold nanorods (GNRs) have attracted much attention because of their high optical absorption peaks in the near-infrared (NIR) region and their effective large-scale preparation.[30-32] It is noted that GNRs has been considered as one of the most efficient exogenous agents for NIR-induced PTT of cancers, showing high efficacy in the ablation of cancer cells *in vitro* and tumors *in vivo*.[33-36] These properties have given rise to many exciting possibilities to employ GNRs for NIR-resonant biomedical imaging, PTT, as well as gene/drug delivery.[37-42] In addition, GNRs have already been used in clinical trials as a thermal agent for cancer therapy.[43, 44]

Recently, bovine serum albumin (BSA), a commercial member of albumin family, was used in synthesis of biomaterials for biomedical applications, owing to its good water solubility, salt tolerance, thermal stability, and excellent biocompatibility.[45-48] Herein, we designed

BSA-bioinspired GNRs loaded with R837 immunoadjuvant for melanoma treatment by combining PTT and immunotherapy. The designed *m*PEG-GNRs@BSA/R837 possessing excellent cytocompatibility and photothermal stability could directly destroy tumor through NIR-induced PTT and trigger a strong immune response with the help of loaded immunoadjuvant *in vitro* and *in vivo*. More importantly, the nanocomplexes under NIR irradiation were able to prevent the lung metastasis and induce a strong long-term immune memory against tumor rechallenge.

## Experimental

### Materials

Cetyltrimethylammonium bromide (CTAB) coated gold nanorods (CTAB-GNRs, 1064 nm), bovine serum albumin (BSA, MW = 66,463), and imiquimod (R837) were purchased from Sigma-Aldrich (St. Louis, MO). Polyethylene glycol (PEG) monomethyl ether with sulfhydryl end group (*m*PEG-SH, Mw = 2000) was from Shanghai Yanyi Biotechnology Corporation (Shanghai, China). CellTiter 96® AQueous one solution cell proliferation assay was from Promega company (Madison, MI). Dulbecco's modified Eagle medium (DMEM), fetal bovine serum (FBS), 0.25% Trypsin-EDTA, penicillin, and streptomycin were purchased from Gibco (Grand Island, NY).

### Synthesis of *m*PEG-GNRs@BSA/R837

*m*PEG-SH (10 mg, 5 mL water) was added into CTAB-GNRs solution ([Au] = 100 μg/mL, 10 mL) under stirring for 24 h, and centrifuged at 10,000 rmp for 15 min to form *m*PEG-GNRs. Then, BSA (10 mg, 5 mL PBS) was mixed with *m*PEG-GNRs ([Au] = 1 mg/mL, 1 mL PBS) under stirring for 2 h to form BSA coated *m*PEG-GNRs (*m*PEG-GNRs@BSA). Lastly, R837 loading was through electrostatic adsorption between positive charge of R837 and negative charge of *m*PEG-GNRs@BSA. In brief, R837 (0.3 mg, 1 mL methanol) was added into *m*PEG-GNRs@BSA ([Au] = 100 μg/mL, 10 mL PBS) under open stirring overnight to volatilize the remaining methanol. Then, the mixture was centrifuged (10,000 rmp) for 15 min to remove the unloaded R837 and washed with deionized water one time to form the final product of *m*PEG-GNRs@BSA/R837.

### *In vitro* cytokine secretion detection

DC2.4 cells were under treatment with either PBS, *m*PEG-GNRs@BSA, *m*PEG-GNRs@BSA/R837, or R837 ([Au] = 11.5 μg/mL, [R837] = 2 μg/mL) for 24 h. DC activated cytokines, such as tumor necrosis factor α (TNF-α), as well as interleukin 6 and 12 (IL-6 and IL-12), were measured by standard enzyme-linked immunosorbent assay (ELISA). Bone-marrow-derived dendritic cells (BMDCs) were also exposed to PBS, *m*PEG-GNRs@BSA, *m*PEG-GNRs@BSA/R837, or R837 ([Au] = 11.5 μg/mL, [R837] = 2 μg/mL) for 24 h. Then the BMDCs were stained with anti-CD40-PacBlue before measurement by flow cytometry (Becton Dickinson; New York, NY).

### Detection adenosine triphosphate (ATP) release assay *in vitro*

B16-F10 cells ($2.5\times10^5$ per well) were seeded in six-well plates for overnight, and then treated with either PBS, *m*PEG-GNRs@BSA/R837 ([Au] = 11.5 μg/mL), laser irradiation

(1.0 W/cm$^2$, 10 min), or *m*PEG-GNRs@BSA/R837 ([Au] = 11.5 μg/mL) plus laser irradiation (1.0 W/cm$^2$, 10 min). After 24 h, the supernatants were collected and cleared from dying tumor cells by centrifugation (2000 rmp, 3 min). Intracellular ATP levels were tested by ATP assay kits (Calbiochem, Nottingham, UK) according to the manufacture's instruction.

### Animal model

All animal procedures were performed in accordance with the Guidelines for Care and Use of Laboratory Animals published by the US National Institutes of Health (NIH) and approved by the University of Oklahoma Health Sciences Center (OUHSC) Institutional Animal Care and Use Committee (IACUC). C57/BL6 mice (six to eight weeks) were purchased from Charles River (Wilmington, MA) and used under protocols approved by OUHSC. B16-F10 cells ($2 \times 10^5$ in 0.1 mL PBS solution) were subcutaneously injected into the right flank of each mouse. The animals were divided into 4 groups (n = 5 for each group) randomly when tumor volumes reached 100-200 mm$^3$. These mice were treated with either PBS (100 μL), *m*PEG-GNRs@BSA/R837 ([Au] = 300 μg/mL, 100 μL) without laser irradiation, laser irradiation (1.0 W/cm$^2$, 10 min), or *m*PEG-GNRs@BSA/R837 ([Au] = 300 μg/mL, 100 μL) plus laser irradiation (1.0 W/cm$^2$, 10 min). Cytokine release in serum of the representative mice from each of established groups was analyzed 3 days after treatment using ELISA. To study tumor weight change and lung metastases, these mice were first injected with India ink through the trachea, and then sacrificed to harvest their tumors and lungs 15 days after treatment. Formation of tumor metastasis regions as white nodules on the surface of black lungs was observed under a microscope.

Survival of treated tumor-bearing mice was monitored. Once tumor volumes reached 100-200 mm$^3$, the mice were divided randomly into 6 groups (n = 10 for each group). These mice were treated with either PBS (100 μL, as a control), *m*PEG-GNRs@BSA/R837 ([Au] = 300 μg/mL, 100 μL), laser irradiation alone (1.0 W/cm$^2$, 10 min), *m*PEG-GNRs@BSA/R837 ([Au] = 300 μg/mL, 100 μL) plus laser irradiation (1.0 W/cm$^2$, 10 min), anti-PD1 inhibitor, or *m*PEG-GNRs@BSA/R837 based PTT in combination with anti-PD1 inhibitor. The survival rate was measured for 100 days since the tumor inoculation. Survivors after treatments and age-matched healthy mice were injected with $2 \times 10^5$ B16-F10 cells into their left flanks of mice (n = 5 for each group). These rechallenged mice were also observed for 100 days.

### Statistical analysis

Statistical analysis was performed via one-way ANOVA statistical method described in our previous work (*p < 0.05, **p < 0.01, ***P < 0.001, respectively).[49, 50]

## Results and discussion

### Construction and characterization of *m*PEG-GNRs@BSA/R837

The *m*PEG-GNRs@BSA/R837 was synthesized beginning with the preparation of *m*PEG-GNRs cores followed by coating BSA protein and loading with R837 through electrostatic

binding (Scheme 1). The BSA-bioinspired *m*PEG-GNRs@BSA/R837 were then used in PTT and immunotherapy for the treatment of melanoma.

Various techniques were utilized to characterize *m*PEG-GNRs@BSA/R837. Transmission electron microscopy (TEM) images revealed that *m*PEG-GNRs@BSA/R837 displayed a uniform size with an average diameter of 122.1 ± 11.6 nm (Fig. 1a). Ultraviolet-visible-NIR (UV-Vis-NIR) spectrometer was used to confirm the formation of GNRs and R837 loading, where *m*PEG-GNRs@BSA and *m*PEG-GNRs@BSA/R837 both showed a typical absorbance band around 1064 nm that belongs to GNRs (Fig. 1b). In addition, after R837 loading, compared to *m*PEG-GNRs@BSA (without R837 loading), two new absorption peaks at 310-330 nm appeared, which were the characteristic absorption peaks of R837 (Fig. S1, ESI†). This result showed that R837 was successfully loaded on GNRs. The surface zeta potentials of CTAB-GNRs and *m*PEG-GNRs were measured to be 57.77 ± 2.93 mV and 12.67 ± 1.52 mV, respectively (Fig. 1c). These results demonstrated that *m*PEG molecules could partly replace positive CTAB. After the surface of *m*PEG-GNRs was coated with negative BSA protein, the zeta potential of *m*PEG-GNRs@BSA was reversed to be −17.77 ± 0.82 mV (Fig. 1c). Finally, the zeta potential of *m*PEG-GNRs@BSA/R837 increased to −12.41 ± 0.12 mV after loading positive R837 (Fig. 1c). The difference in zeta potential between *m*PEG-GNRs and *m*PEG-GNRs@BSA was the evidence of BSA coating. Furthermore, R837 drug showing positive charge was successfully loaded on GNRs surface through electrostatic adsorption (Fig. 1b), also confirming the negative charge of the GNRs after BSA coating. The loading efficiency of R837 on *m*PEG-GNRs@BSA/R837 was measured to be 57.84% according to the standard calibration curve (Fig. S1, ESI†). The R837 release profiles in *m*PEG-GNRs@BSA/R837 were investigated separately in two different pH conditions (Fig. S2, ESI†). We found that R837 was slowly released from the nanocomplexes in a pH-dependent manner. The R837 release rate was 64.77 ± 7.3% under the acidic condition (pH 5.0), and was 23.35 ± 2.1% under the physiological condition (pH 7.4) after 65 h incubation at 37 °C. The faster R837 release under acidic condition is likely because a majority of R837 is protonated and displays high water solubility under this condition. Furthermore, the designed *m*PEG-GNRs@BSA/R837 displayed an excellent colloidal stability for at least 7 days after they were dispersed in water, PBS or cell-culture medium at 4 °C (Fig. S3, ESI†).

To evaluate the photothermal properties of *m*PEG-GNRs@BSA/R837, the nanocomplexes were exposed to a 1064 nm laser (1.0 W/cm$^2$) at different concentrations for 10 min. As shown in Fig. 1d, with the increase of Au concentration, the temperatures of the nanocomplexes continued to rise under laser irradiation. The temperature of the nanocomplexes with high Au concentration (20 μg/mL) reached 60°C, whereas the temperature only up to 38.9 °C by water + laser irradiation (Fig. 1d). These results indicated that *m*PEG-GNRs@BSA/R837 was able to convert NIR light into thermal energy rapidly and efficiently. The photothermal stability of *m*PEG-GNRs@BSA/R837 was further evaluated. We monitored the temperature of *m*PEG-GNRs@BSA/R837 ([Au] = 10 μg/mL) solution under laser irradiation, followed by natural cooling to room temperature (Fig. S4, ESI†). Our results showed that the photothermal effect of the nanocomplexes did not suffer from any attenuation after repeated laser on/off cycles, suggesting that the nanocomplexes possessed a desirable photothermal stability.

## Cytotoxicity assay

The cytotoxicity of *m*PEG-GNRs@BSA was examined *via* 3-(4,5-dimethylthiazol-2-yl)-5-(3-carboxymethoxyphenyl)-2-(4-sulfophenyl)-2H-tetrazolium (MTS) assay (Fig. 2a) and morphology observation (Fig. S5, ESI†) of B16-F10 cells co-cultured with the nanocomplexes at different concentrations. It was clear that the cell viability and morphology after being treated with the nanocomplexes ([Au] = 0-100 μM) were approximately similar to that of the PBS control. These results verified that the nanocomplexes had no apparent cytotoxicity in the given concentration range.

We next evaluated the *in vitro* PTT of *m*PEG-GNRs@BSA nanocomplexes. We found that the cell viability decreased to 27.4% after an incubation with 11.5 μg Au/mL of the complexes and exposure to the NIR laser irradiation at the power density of 0.85 W/cm$^2$, whereas, the cell viability was 83.5% under laser irradiation alone at the same condition (Fig. 2b). Meanwhile, the live and dead cells were stained with green fluorescence related to calcein AM (live cells) and red fluorescence related to propidium iodide (PI, dead cell), as shown in Fig. 2c. Most of the cells were killed after treatment with the complexes ([Au] = 100 μM) under the 1064 nm laser irradiation for 10 min, consistent with MTS data. This implied a high PTT efficiency when used with the nanocomplexes in inducing cancer cell death.

## *In vitro* cytokine secretion detection

DCs are antigen-presenting cells for activating native T cells. Immature DCs uptake antigens in the surrounding tumor environment, and process them into peptides during migration for T cell activation. The immune-related cell cytokines from DCs, including TNF-α (a key marker in the activation of cellular immunity), as well as IL-6 and IL-12 (key markers of innate immunity), were measured by ELISA. We found that an apparent enhancement in the secretion levels of TNF-α, IL-6, and IL-12 after treatment with free R837 and *m*PEG-GNRs@BSA/R837 (Fig. 3a). Moreover, no significant difference in secretion enhancements between the free R837 and *m*PEG-GNRs@BSA/R837 was observed ($p > 0.5$). In addition, no obvious secretion enhancement was observed after treatment with PBS control and *m*PEG-GNRs@BSA. Therefore, the designed *m*PEG-GNRs@BSA/R837 could cause a strong immune response. Meanwhile, BMDCs were harvested and treated with either *m*PEG-GNRs@BSA, *m*PEG-GNRs@BSA/R837, or free R837 for 24 h. The percentage of mature DCs (CD40) was measured by flow cytometry (Fig. 3b). We found that the percentages of mature DCs treated with *m*PEG-GNRs@BSA/R837 increased significantly (65.1%), similar to that of the treatment of free R837 (60%), whereas the percentages of mature DCs treated with *m*PEG-GNRs@BSA without R837 remained at 37.9%, similar to that of PBS control (34.9%). Our data further indicated the strong immune stimulation by *m*PEG-GNRs@BSA/R837.

## Immunogenic cell death

Immunogenic cell death was measured by the post-apoptotic release of the HSP70/β-Actin protein and ATP. As shown in Fig. 4, B16-F10 cells treated with *m*PEG-GNRs@BSA/R837 plus laser irradiation or laser irradiation alone displayed much higher HSP70/β-Actin release than that with PBS or *m*PEG-GNRs@BSA/R837 (Fig. 4a). Interestingly, the HSP70/β-Actin

release from cells treated with *m*PEG-GNRs@BSA/R837 plus laser irradiation was higher than that with laser irradiation alone (Fig. 4b). In addition, the B16-F10 cells treated with *m*PEG-GNRs@BSA/R837 plus laser irradiation could significantly enhance the ATP release (Fig. 4c), corroborating the HSP70/β-Actin release data.

### *In vivo* antitumor efficacy

We further evaluated the *in vivo* antitumor efficacy of *m*PEG-GNRs@BSA/R837 under laser irradiation using a B16-F10 tumor model in comparison with *m*PEG-GNRs@BSA/R837 (without laser irradiation) and laser irradiation alone. PBS was used as control. First, the changes of different cytokines in serum, including TNF-α, IL-6, and IL-12, were measured by ELISA after various treatments for 3 days. As shown in Fig. 5a, the secretion level of TNF-α from mouse tumor treated with *m*PEG-GNRs@BSA/R837 plus laser irradiation was higher than that of other treatments. A significant up-regulation of IL-6 and IL-12 was also observed after the treatment of *m*PEG-GNRs@BSA/R837-PTT (Fig. 5a). Therefore, the nanocomplex-based PTT could induce apparently immunological response *in vivo*, which constituted to the prerequisite for combination of PTT and immunotherapy *in vivo*. The macrophage activation was further evaluated by TNF-α release from B16-F10 tumor using ELISA. We found that the B16-F10 tumor treated with *m*PEG-GNRs@BSA/R837 under irradiation by a 1064 nm NIR laser could significantly enhance TNF-α release of the macrophages (Fig. 5b). Quantitative TNF-α release after different treatments followed the order of *m*PEG-GNRs@BSA/R837 plus laser irradiation > R837 plus laser irradiation > *m*PEG-GNRs@BSA plus laser irradiation > laser irradiation alone > PBS (Fig. 5b). Our data revealed a strong ability of the R837-loaded *m*PEG-GNRs@BSA/R837-PTT in enhancement immunological responses.

Lastly, *m*PEG-GNRs@BSA/R837-PTT had obvious advantages in inhibiting tumor growth, compared with other treatments (Fig. 5c). Additionally, hematoxylin and eosin (H&E) staining of tumor slices also confirmed that the majority of tumor cells were damaged by *m*PEG-GNRs@BSA/R837-PTT (Fig. 5f), when compared with PBS (Fig. 5d) or laser irradiation (Fig. 5e) group. This could be mainly due to the fact that the GNRs based PTT killed tumor cells in part, which can act as tumor-related antigens; then these antigens can be processed and presented by antigen-presenting cells to activate and elicit the proliferation of tumor-specific effector T cells in lymphoid organs with the aid of R837 immunoadjuvant; finally, these activated T cells could attack tumor cells and metastatic tumor cells. This process was vividly depicted in Scheme 1. This process was further verified by an immunofluorescence staining assay. As shown in Fig. 6, DCs (CD11c, red fluorescence) were significantly increased in tumor-bearing mice one day after treatment with *m*PEG-GNRs@BSA/R837 plus laser irradiation, compared with laser irradiation alone. Meanwhile, seven days after treatments, *m*PEG-GNRs@BSA/R837 plus laser irradiation effectively enhanced the $CD8^+$ T cells infiltration (red fluorescence, Fig. 6). The *in situ* 1064-nm GNRs and the non-invasive irradiation by a 1064-nm laser provided a perfect selective photothermal interaction. Only the target tissue containing the 1064-nm GNRs will experience the desirable temperature increase to induce tumor cell death and tumor antigen release. The advantages of the 1064-nm laser-GNR combination are reflected by the significant temperature increase, significant cell and tumor death (Fig. 2b and Fig. 5f).

We next evaluated the inhibition of metastases in the lungs. We found that *m*PEG-GNRs@BSA/R837 plus laser irradiation was more effective in preventing lung metastases 15 days after treatment than other treatments (Fig. S6, ESI†). The number of B16-F10 lung metastases in mice treated by *m*PEG-GNRs@BSA/R837 plus laser irradiation was only 55.6, which was much less than other treatments (e.g., 152.8 of PBS, 119.8 of *m*PEG-GNRs@BSA/R837 without laser irradiation, and 110 of laser irradiation alone).

During the studied time of 100 days, as given in Fig. 7a, the survival rate was highest with *m*PEG-GNRs@BSA/R837 plus laser irradiation, where seven of ten mice survived. With laser irradiation alone, two of ten mice survived, and with both *m*PEG-GNRs@BSA/R837 and PBS, no mice survived. These results further confirmed the enhanced antitumor effect of *m*PEG-GNRs@BSA/R837-PTT and immunotherapy that can effectively inhibit tumor metastases. It is well known that targeting T cell inhibitory checkpoint signaling pathways has provided a promising strategy for tumor-specific immunotherapy.[19, 51] FDA approved checkpoint inhibitors such as anti-CTLA-4 and anti-PD-1 can modulate immunosuppressive environments within tumors. The combination of these checkpoint inhibitors with other types of treatment strategies could offer additional therapeutic benefits in cancer treatment. It was found that the anti-PD-1 inhibitor alone had a limited effect on the long-term survival, whereas *m*PEG-GNRs@BSA/R837-PTT plus anti-PD-1 inhibitor could significantly increase the animal survival rate, as evidenced by the survival of eight in ten mice (Fig. 7a). This result indicated that tumors were sensitized to anti-PD-1 inhibitor, and *m*PEG-GNRs@BSA/R837-PTT in combination with anti-PD-1 inhibitor induced a strong synergistic antitumor immunological effect. This could cause by the fact that anti-PD-1 inhibitor can block PD-1 signaling pathway of T cells, and inhibit the activities of immune-suppressive regulatory T cells, which showed in Scheme 1.

### Recurrence assay *in vivo*

We further evaluated long-term immunity induced by *m*PEG-GNRs@BSA/R837-PTT. As shown in Fig. 7b, the mice treated by *m*PEG-GNRs@BSA/R837-PTT could significantly inhibit the growth of re-inoculated tumor; all the mice survived more than 100 days after the second tumor inoculation. In sharp contrast, no mice survived in the age-matched group or in the laser alone group. These results demonstrated a strong long-term immune memory induced by *m*PEG-GNRs@BSA/R837-PTT to protect mice from tumor recurrence. The enhanced antitumor effect by combined PTT and immunotherapy rely on the synergistic effects of PTT and immunological stimulation. PTT, by delivering sufficient thermal energy to target tumor tissue, kills tumor cells and, at the same time, releases tumor-specific antigens. Immunological therapy, through local application of R837 in this study, combines the exposed tumor antigens to activate, enhance, and direct the host immune system to establish a tumor-specific immunity. This synergy has been demonstrated by our previous results.[22, 29] It is also supported by our current study, as shown by the results in Fig. 5 and Fig. 7.

## Conclusions

In summary, we developed BSA inspired gold nanorods loaded with immunoadjuvant for combined photothermal therapy and immunotherapy for treatment of melanoma. The designed *m*PEG-GNRs@BSA/R837 are cytocompatible and colloidally/photothermally stable. They can directly destroy tumor through NIR-induced PTT and trigger strong immune response with the help of loaded immunoadjuvant *in vitro* and *in vivo*. More importantly, *m*PEG-GNRs@BSA/R837 under NIR laser irradiation could inhibit lung metastasis and induce a strong long-term antitumor immunity to prevent tumor recurrence. We believe the combination of PTT and immunotherapy using the BSA-bioinspired GNRs loaded with immunoadjuvant holds great potential for treatment of melanoma in clinical settings.

## Supplementary Material

Refer to Web version on PubMed Central for supplementary material.

## Acknowledgements

This research is supported by the U.S. National Institutes of Health (RS20132225-106, R21 EB 015509-01, and R01CA205348-01), the Oklahoma Center for the Advancement of Science and Technology (HR16-085), the National Natural Science Foundation of China (61805161 and 61705143), the China Postdoctoral Science Foundation (2017M622766, 2018T110890, and 2018M630979), and the Shenzhen Basic Research Project (JCYJ20170818143045740).

## Notes and references

1. Siegel RL, Miller KD and Jemal A, Ca-Cancer J. Clin, 2017, 67, 7–30. [PubMed: 28055103]
2. DeSantis CE, Lin CC, Mariotto AB, Siegel RL, Stein KD, Kramer JL, Alteri R, Robbins AS and Jemal A, Ca-Cancer J. Clin, 2014, 64, 252–271. [PubMed: 24890451]
3. Finn L, Markovic SN and Joseph RW, BMC Med, 2012, 10, 23. [PubMed: 22385436]
4. Drake CG, Lipson EJ and Brahmer JR, Nat. Rev. Clin. Oncol, 2014, 11, 24–37. [PubMed: 24247168]
5. Kuai R, Ochyl LJ, Bahjat KS, Schwendeman A and Moon JJ, Nat. Mater, 2017, 16, 489–496. [PubMed: 28024156]
6. Ott PA, Hu Z, Keskin DB, Shukla SA, Sun J, Bozym DJ, Zhang W, Luoma A, Giobbie-Hurder A, Peter L, Chen C, Olive O, Carter TA, Li S, Lieb DJ, Eisenhaure T, Gjini E, Stevens J, Lane WJ, Javeri I, Nellaiappan K, Salazar AM, Daley H, Seaman M, Buchbinder EI, Yoon CH, Harden M, Lennon N, Gabriel S, Rodig SJ, Barouch DH, Aster JC, Getz G, Wucherpfennig K, Neuberg D, Ritz J, Lander ES, Fritsch EF, Hacohen N and Wu CJ, Nature, 2017, 547, 217–221. [PubMed: 28678778]
7. Azijli K, Stelloo E, Peters GJ and Van den Eertwegh AJ, Anticancer Res, 2014, 34, 1493–1505. [PubMed: 24692676]
8. Wei SC, Levine JH, Cogdill AP, Zhao Y, Anang N, Andrews MC, Sharma P, Wang J, Wargo JA, Pe'er D and Allison JP, Cell, 2017, 170, 1120–1133. [PubMed: 28803728]
9. Pardoll DM, Nat. Rev. Cancer, 2012, 12, 252–264. [PubMed: 22437870]
10. Sharma P and Allison JP, Science, 2015, 348, 56–61. [PubMed: 25838373]
11. Wang C, Ye YQ, Hochu GM, Sadeghifar H and Gu Z, Nano Lett, 2016, 16, 2334–2340. [PubMed: 26999507]
12. Luke JJ, Flaherty KT, Ribas A and Long GV, Nat. Rev. Clin. Oncol, 2017, 14, 463–482. [PubMed: 28374786]

13. Johnson DB, Peng C and Sosman JA, Ther. Adv. Med. Oncol, 2015, 7, 97–106. [PubMed: 25755682]
14. Herndon TM, Demko SG, Jiang XP, He K, Gootenberg JE, Cohen MH, Keegan P and Pazdur R, Oncologist, 2012, 17, 1323–1328. [PubMed: 23002124]
15. Chen Q, Xu LG, Chen JW, Yang ZJ, Liang C, Yang Y and Liu Z, Biomaterials, 2017, 148, 69–80. [PubMed: 28968536]
16. Liang C, Xu LG, Song GS and Liu Z, Chem. Soc. Rev, 2016, 45, 6250–6269. [PubMed: 27333329]
17. Tao Y, Ju EG, Liu Z, Dong K, Ren JS and Qu XG, Biomaterials, 2014, 35, 6646–6656. [PubMed: 24818880]
18. Wang D, Wang T, Liu J, Yu H, Jiao S, Feng B, Zhou F, Fu Y, Yin Q, Zhang P, Zhang Z, Zhou Z and Li Y, Nano Lett, 2016, 16, 5503–5513. [PubMed: 27525587]
19. Min YZ, Roche KC, Tian SM, Eblan MJ, McKinnon KP, Caster JM, Chai SJ, Herring LE, Zhang LZ, Zhang T, DeSimone JM, Tepper JE, Vincent BG, Serody JS and Wang AZ, Nat. Nanotechnol, 2017, 12, 877–882. [PubMed: 28650437]
20. Pan JB, Wang YQ, Zhang C, Wang XY, Wang HY, Wang JJ, Yuan YZ, Wang X, Zhang XJ, Yu CS, Sun SK and Yan XP, Adv. Mater, 2018, 30, 1704408.
21. He CB, Duan XP, Guo NN, Chan C, Poon C, Weichselbaum RR and Lin WB, Nat. Commun, 2016, 7, 12499. [PubMed: 27530650]
22. Chen WR, Liu H, Ritchey JW, Bartels KE, Lucroy MD and Nordquist RE, Cancer Res, 2002, 62, 4295–4299. [PubMed: 12154032]
23. Duan XP, Chan C, Guo NN, Han WB, Weichselbaum RR and Lin WB, J. Am. Chem. Soc, 2016, 138, 16686–16695. [PubMed: 27976881]
24. Wang ZJ, Fu Y, Kang ZZ, Liu XG, Chen N, Wang Q, Tu YQ, Wang LH, Song SP, Ling DS, Song HY, Kong XQ and Fan CH, J. Am. Chem. Soc, 2017, 139, 15784–15791. [PubMed: 29024595]
25. Xu J, Xu LG, Wang CY, Yang R, Zhuang Q, Han X, Dong ZL, Zhu WW, Peng R and Liu Z, ACS Nano, 2017, 11, 4463–4474. [PubMed: 28362496]
26. Yata T, Takahashi Y, Tan MM, Nakatsuji H, Ohtsuki S, Murakami T, Imahori H, Umeki Y, Shiomi T, Takakura Y and Nishikawa M, Biomaterials, 2017, 146, 136–145. [PubMed: 28918263]
27. Zhou B, Xiong Z, Wang P, Peng C, Shen M, Mignani S, Majoral J-P and Shi X, Drug Delivery, 2018, 25, 178–186. [PubMed: 29301434]
28. Chen Q, Xu LG, Liang C, Wang C, Peng R and Liu Z, Nat. Commun, 2016, 7, 13193. [PubMed: 27767031]
29. Zhou F, Wu S, Song S, Chen WR, Resasco DE and Xing D, Biomaterials, 2012, 33, 3235–3242. [PubMed: 22296829]
30. Huang X, Neretina S and El-Sayed MA, Adv. Mater, 2009, 21, 4880–4910. [PubMed: 25378252]
31. Zhou J, Cao ZL, Panwar N, Hu R, Wang XM, Qu JL, Tjin SC, Xu GX and Yong KT, Coord. Chem. Rev, 2017, 352, 15–66.
32. Grzelczak M, Perez-Juste J, Mulvaney P and Liz-Marzan LM, Chem. Soc. Rev, 2008, 37, 1783–1791. [PubMed: 18762828]
33. Zhang L, Su HL, Cai JL, Cheng DF, Ma YJ, Zhang JP, Zhou CQ, Liu SY, Shi HC, Zhang YJ and Zhang CF, ACS Nano, 2016, 10, 10404–10417. [PubMed: 27934087]
34. Choi J, Yang J, Bang D, Park J, Suh JS, Huh YM and Haam S, Small, 2012, 8, 746–753. [PubMed: 22271594]
35. Qiu JJ and Wei WD, J. Phys. Chem. C, 2014, 118, 20735–20749.
36. Choi WI, Kim JY, Kang C, Byeon CC, Kim YH and Tee G, ACS Nano, 2011, 5, 1995–2003. [PubMed: 21344891]
37. Sun MZ, Xu LG, Ma W, Wu XL, Kuang H, Wang LB and Xu CL, Adv. Mater, 2016, 28, 898–904. [PubMed: 26635317]
38. Xu WJ, Qian JM, Hou GH, Suo AL, Wang YP, Wang JL, Sun TT, Yang M, Wan XL and Yao Y, ACS Appl. Mater. Interfaces, 2017, 9, 36533–36547. [PubMed: 28975790]
39. Zeng JY, Zhang MK, Peng MY, Gong D and Zhang XZ, Adv. Funct. Mater, 2018, 28, 1705451.

40. Zhang ZJ, Wang J, Nie X, Wen T, Ji YL, Wu XC, Zhao YL and Chen CY, J. Am. Chem. Soc, 2014, 136, 7317–7326. [PubMed: 24773323]
41. Lee C, Hwang HS, Lee S, Kim B, Kim JO, Oh KT, Lee ES, Choi HG and Youn YS, Adv. Mater, 2017, 29, 1605563.
42. Wang BK, Yu XF, Wang JH, Li ZB, Li PH, Wang HY, Song L, Chu PK and Li CZ, Biomaterials, 2016, 78, 27–39. [PubMed: 26646625]
43. Davis ME, Zuckerman JE, Choi CHJ, Seligson D, Tolcher A, Alabi CA, Yen Y, Heidel JD and Ribas A, Nature, 2010, 464, 1067–1070. [PubMed: 20305636]
44. Libutti SK, Paciotti GF, Byrnes AA, Alexander HR, Gannon WE, Walker M, Seidel GD, Yuldasheva N and Tamarkin L, Clin. Cancer Res, 2010, 16, 6139–6149. [PubMed: 20876255]
45. Cobo I, Li M, Sumerlin BS and Perrier S, Nat. Mater, 2015, 14, 143–159. [PubMed: 25401924]
46. Yang WT, Guo WS, Le WJ, Lv GX, Zhang FH, Shi L, Wang XL, Wang J, Wang S, Chang J and Zhang BB, ACS Nano, 2016, 10, 10245–10257. [PubMed: 27791364]
47. Guo Z, Zhu S, Yong Y, Zhang X, Dong XH, Du JF, Xie JN, Wang Q, Gu ZJ and Zhao YL, Adv. Mater, 2017, 29, 1704136.
48. Gao FP, Cai PJ, Yang WJ, Xue JQ, Gao L, Liu R, Wang YL, Zhao YW, He X, Zhao LN, Huang GD, Wu FS, Zhao YL, Chai ZF and Gao XY, ACS Nano, 2015, 9, 4976–4986. [PubMed: 25919205]
49. Zhou B, Wang R, Chen F, Zhao L, Wang P, Li X, Banyai I, Ouyang Q, Shi X and Shen M, ACS Appl. Mater. Interfaces, 2018, 10, 6146–6154. [PubMed: 29380596]
50. Zhou B, Zhao L, Shen M, Zhao J and Shi X, J. Mater. Chem. B, 2017, 5, 1542–1550.
51. Chiang C-S, Lin Y-J, Lee R, Lai Y-H, Cheng H-W, Hsieh C-H, Shyu W-C and Chen S-Y, Nat. Nanotechnol, 2018, 13, 746–754. [PubMed: 29760523]

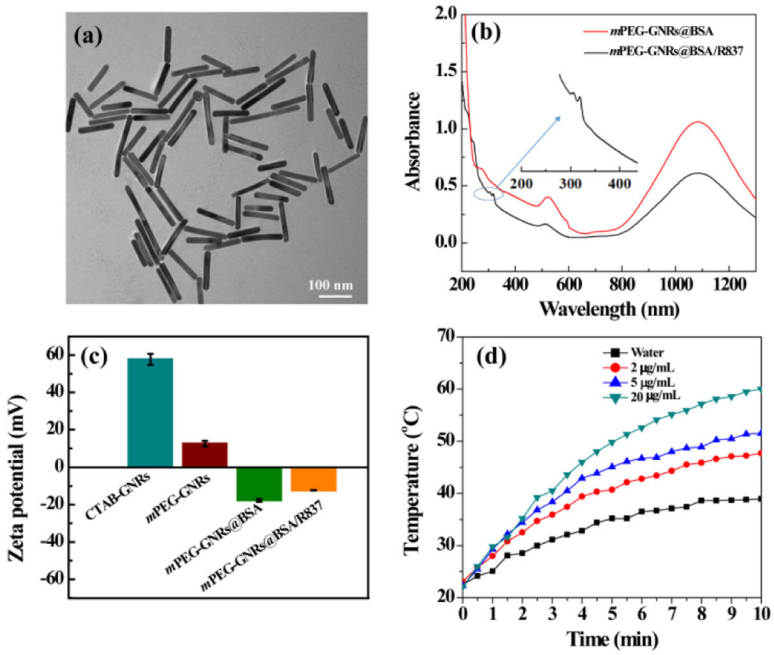


**Fig. 1.**

(a) TEM image of *m*PEG-GNRs@BSA/R837. (b) UV-Vis-NIR spectrum of *m*PEG-GNRs@BSA and *m*PEG-GNRs@BSA/R837 (Inset is the local zoom of UV-Vis-NIR spectrum of *m*PEG-GNRs@BSA/R837). (c) Zeta potential of the CTAB-GNRs, *m*PEG-GNRs, *m*PEG-GNRs@BSA, and *m*PEG-GNRs@BSA/R837, respectively. (d) Photothermal heating curves of water and *m*PEG-GNRs@BSA/R837 dispersed in water at different Au concentrations under a 1064 nm laser irradiation (1.0 W/cm$^2$).

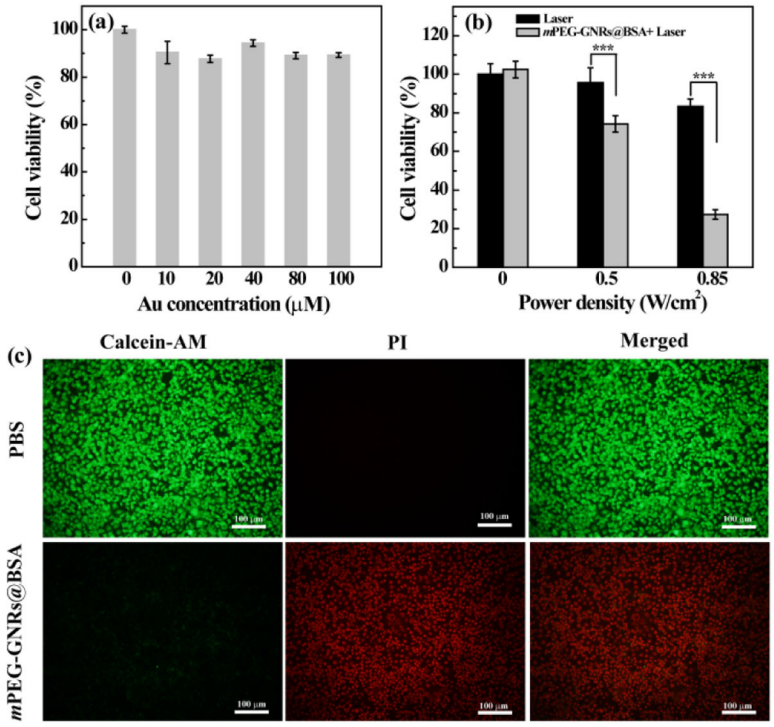


**Fig. 2.**

(a) Cell viability of B16-F10 cells treated with *m*PEG-GNRs@BSA at different concentrations for 24 h. (b) Cell viability of B16-F10 cells treated with *m*PEG-GNRs@BSA at the Au concentration of 58.4 μM for 6 h followed by irradiation with a 1064 nm NIR laser (1.0 W/cm$^2$) for 10 min at different power densities. (c) Fluorescence images of cells treated with PBS and *m*PEG-GNRs@BSA at the Au concentration of 100 μM, and irradiated with a 1064 nm laser at 1.0 W/cm$^2$ for 10 min (calcein-AM stained live cells, PI stained dead cells).

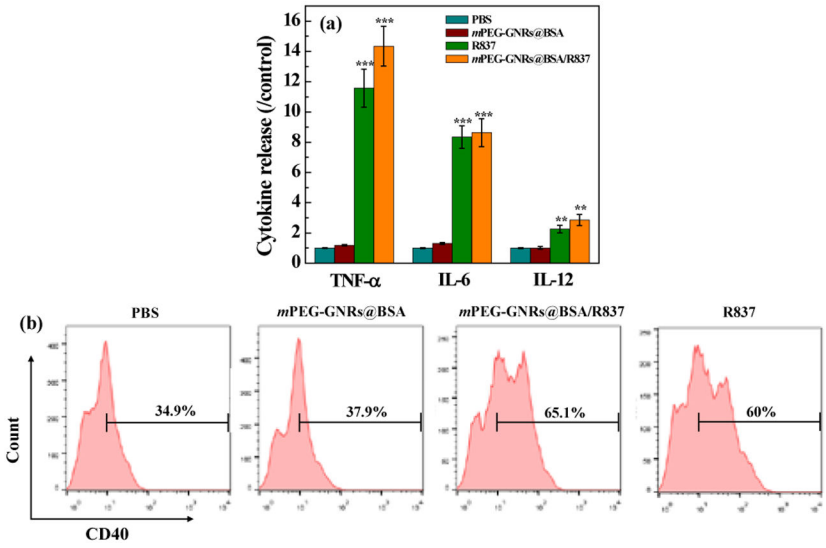


**Fig. 3.**

(a) Cytokine secretion release of TNF-α, IL–6 and IL–12 by DC2.4 cells treated with PBS, *m*PEG-GNRs@BSA, *m*PEG-GNRs@BSA/R837, or R837 ([Au] = 11.5 μg/mL, [R837] = 2 μg/mL) for 24 h (All data were compared with the PBS control). (b) Quantification of CD40 expression in BMDCs after different treatments ([Au] = 11.5 μg/mL, [R837] = 2 μg/mL) for 24 h by flow cytometry.

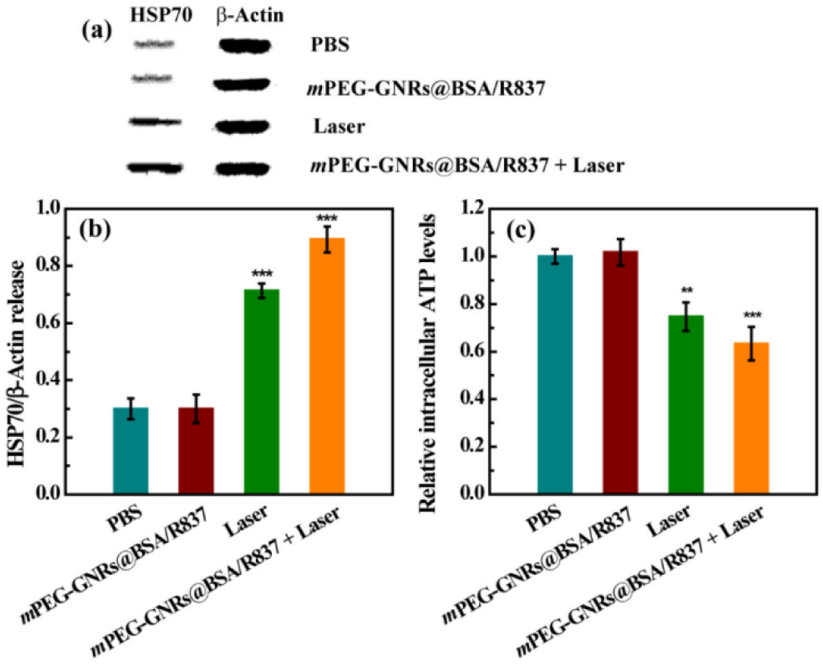


**Fig. 4.**

Western blot assay (a) and quantitative analysis (b) of the expression of HSP70/b-Actin in B16-F10 cells after different treatments for 24 h. (c) Relative intracellular ATP levels in B16-F10 cells after different treatments for 24 h. All data were compared with the PBS control.

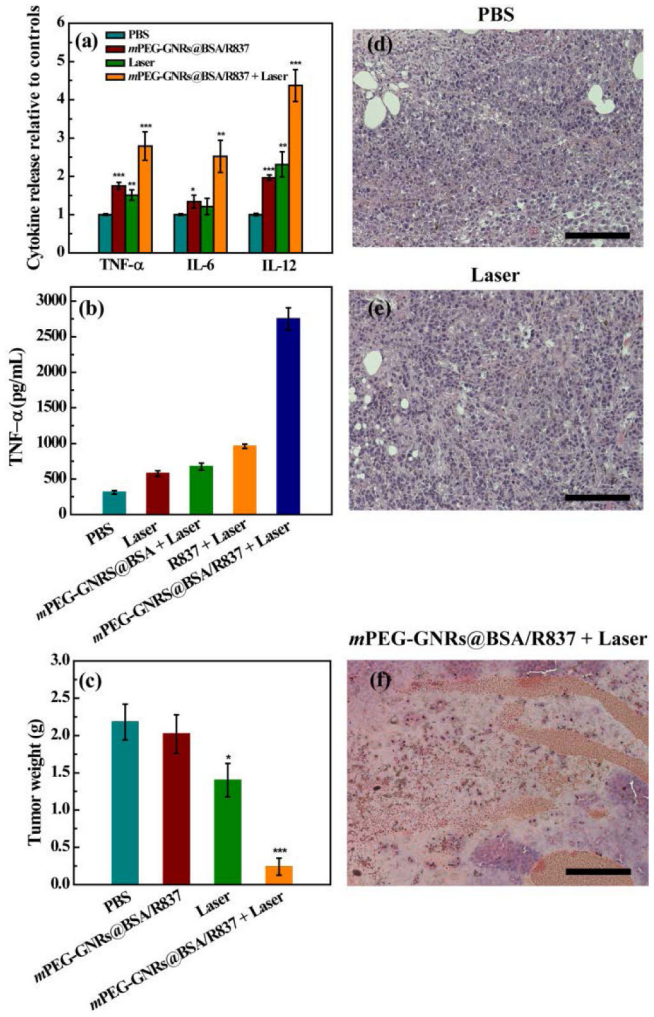


**Fig. 5.**

(a) Cytokine levels of TNF-α, IL-6, and IL-12 in serum of mice 3 days after various treatments. (b) Cytokine secretion of TNF-α from macrophages stimulated by treated B16-F10 tumor after various treatments. (c) Weight of primary tumor 15 days after various treatments. All data were compared with the PBS control. H&E stained tumors one day after treatments by PBS (d), laser irradiation alone (e), and *m*PEG-GNRs@BSA/R837 plus laser irradiation (f). Bar = 100 μm.

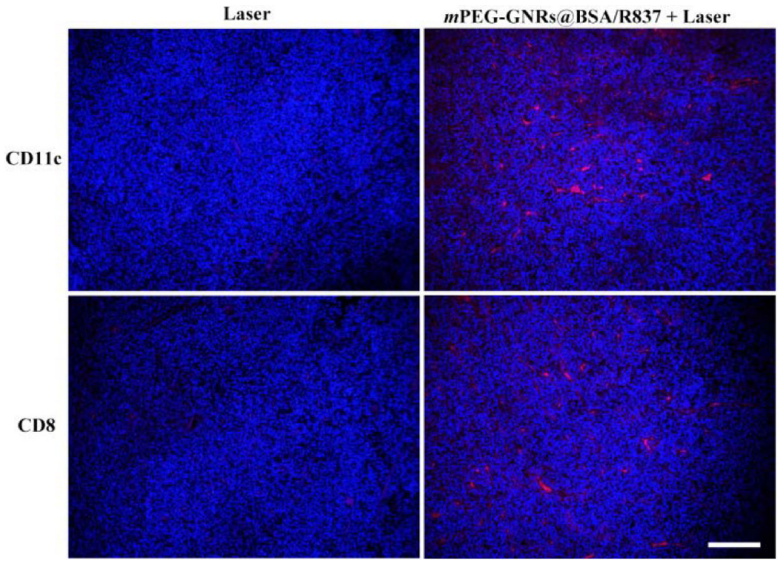


**Fig. 6.**

Representative immunofluorescence staining for CD11c (red) and CD8 (red) of B16-F10 tumor sections obtained at one day (CD11c) or seven days (CD8) after various treatments. The tumor cell nucleus was stained with 4′,6-diamidino-2-phenylindole (DAPI, blue). Bar = 100 μm.

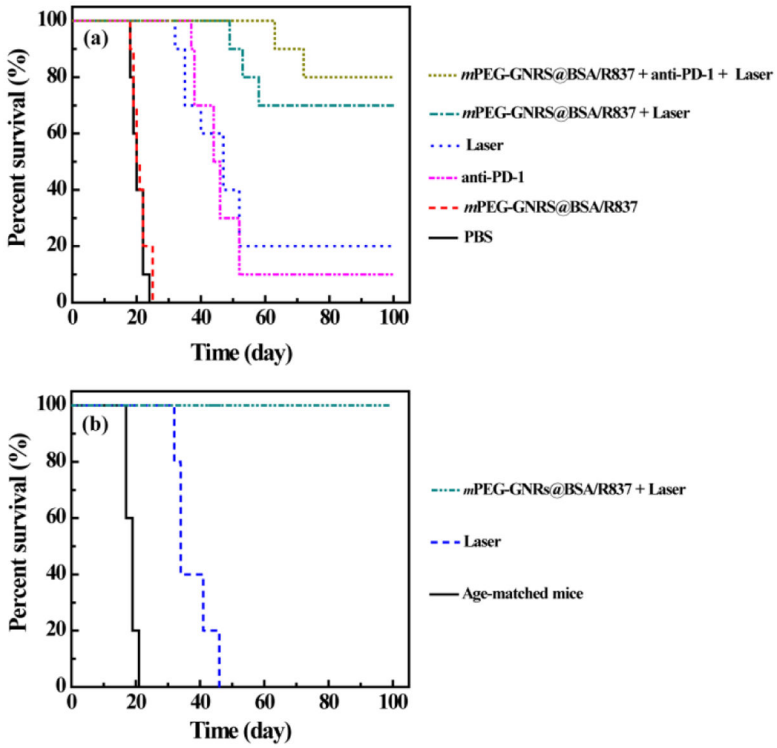


**Fig. 7.**

(a) Survival rates of mice after various treatments as a function of time post tumor inoculation. (b) Survival rates of the re-inoculated tumor-bearing mice after the successful treatment by laser irradiation alone or *m*PEG-GNRs@BSA/R837 plus laser irradiation. Age-matched mice were used as a control.

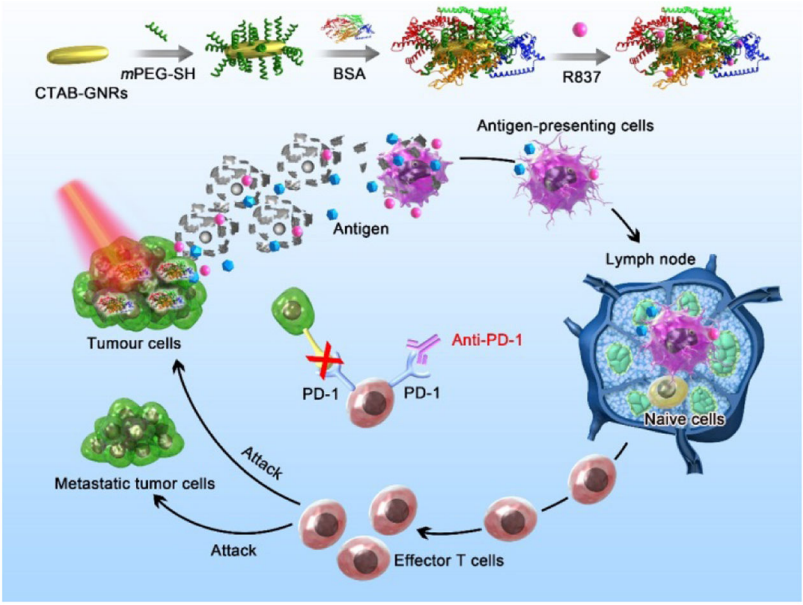


**Scheme 1.**

Schematic illustration of *m*PEG-GNRs@BSA/R837 nanocomplexes and the mechanism of antitumor immune responses trigged by the nanocomplexes.